Tidally-induced variations of pH at the head of the Laurentian Channel

Alfonso Mucci[1], Maurice Levasseur[2], Yves Gratton[3], Chloé Martias[1], Michael Scarratt[4], Denis Gilbert[4], Jean-Éric Tremblay[2], Gustavo Ferreyra[5] and Bruno Lansard[6]

1- GEOTOP and Department of Earth and Planetary Sciences, McGill University, 3450 University Street, Montréal, QC, Canada H3A 0E8
2- Québec-Océan and Département de Biologie, Université Laval, 1045 Avenue de la Médecine, Québec, QC, Canada G1V 2R3
3- Institut national de la Recherche Scientifique, Eau Terre et Environnement, 490 rue de la Couronne, Québec, QC, Canada G1K 9A9
4- Fisheries and Ocean Canada, Maurice Lamontagne Institute, 850 Route de la Mer, Mont-Joli, QC, Canada QC G5H 3Z4
5- Québec-Océans et Institut des Sciences de la Mer de Rimouski, 310 Allée des Ursulines, Rimouski, QC, Canada G5L 3A1
6- Laboratoire des Sciences du Climat et de l'Environnement, avenue de la Terrasse, domaine du CNRS, bât. 12, 91198, Gif-sur-Yvette, France

ABSTRACT

The head of the Laurentian Channel (LC) is a very dynamic region of exceptional biological richness. To evaluate the impact of freshwater discharge, tidal mixing, and biological activity on the pH of surface waters in this region, a suite of physical and chemical variables was measured throughout the water column over two tidal cycles. The relative contributions to the water column of the four source-water types that converge in this region were evaluated using an optimum multi-parameter algorithm (OMP). Results of the OMP analysis were used to reconstruct the water column properties assuming conservative mixing, and the difference between the model properties and field measurements served to identify factors that control the pH of the surface waters. These surface waters are generally undersaturated with respect to aragonite, mostly due to the intrusion of waters from the Upper St. Lawrence Estuary and the Saguenay Fjord. The presence of a cold intermediate layer impedes the upwelling of the deeper, hypoxic, lower pH and aragonite-undersaturated waters of the Lower St. Lawrence Estuary to depths shallower than 50 meters.

RÉSUMÉ

La tête du chenal Laurentien est une région très dynamique d'une richesse biologique exceptionnelle. Afin d'évaluer l'impact des apports en eaux douces, du mélange tidal, et de l'activité biologique sur le pH des eaux de surface dans cette région, une suite de variables physiques et chimiques a été mesurée dans la colonne d'eau sur deux cycles de marée. La contribution relative des quatre sources d'eau-type qui convergent dans cette région a été évaluée à l'aide d'un algorithme d'optimisation multi-paramétrique (OMP). Les résultats de l'OMP ont été utilisés pour reconstruire les propriétés de la colonne d'eau en assumant un mélange conservateur et la différence entre les propriétés issues du modèle et des mesures effectuées sur le terrain ont servies à identifier les facteurs qui contrôlent le pH des eaux de surface. Les eaux de surface sont généralement sous-saturées par rapport à l'aragonite, surtout à cause de l'intrusion d'eau provenant de l'estuaire fluvial du Saint-Laurent et du fjord du Saguenay. La présence de la couche intermédiaire froide (CIF) durant les marées de morte-eau tamponne l'acidification des eaux de surface dans cette région de l'estuaire. La présence d'une couche intermédiaire froide limite la remontée des eaux profondes, hypoxiques, de faible pH et sous-saturées par rapport à l'aragonite de l'estuaire maritime du Saint-Laurent à des profondeurs de moins de 50 mètres.

INTRODUCTION

The oceans have absorbed approximately 30% of the anthropogenic CO_2 released to the atmosphere since the beginning of the industrial revolution (Sabine et al. 2004). Consequently, over the last century, the pH of the global ocean surface has decreased by an estimated 0.1 unit, equivalent to a 30% increase in the proton concentration (Caldeira and Wickett 2005). The increased acidity has lowered the saturation state of ocean waters with respect to calcite and aragonite (the two most common $CaCO_3$ polymorphs that constitute the shells and skeleton of many marine organisms) and, in combination with other stresses such as global warming, likely affected the ecology of carbonate-secreting organisms (Fabry et al. 2008, Miller et al. 2009; Ries et al. 2009; Kroeker et al. 2013) as well as non-calcifiers because pH plays a critical role in mediating many physiological processes (Fabry et al. 2008; Kroeker et al. 2013).

The pH of surface waters in coastal systems is controlled by more dynamic processes than in the open ocean. In these systems, the pH of surface waters may exhibit important short (hours) and long (season) term variations in response to freshwater inputs and vertical mixing (Abril et al. 2000; Feely et al. 2010). Freshwater rivers and inner estuaries are typically supersaturated in CO_2 with respect to the atmosphere (Meybeck 1993; Raymond et al. 1997; Barth et al. 1999; Bauer et al. 2013; Dinauer and Mucci 2017) as a result of inputs from their drainage basin and the activity of heterotrophic organisms sustained by natural or anthropogenic terrestrial and riverine organic carbon inputs (Frankinouille et al. 1996, 1998; Feely et al. 2010). Consequently, waters are often characterized by circum-neutral to slightly acidic pHs (Wallace et al. 2014) and are a net source of CO_2 to the atmosphere (see compilation in Chen and Borges 2009). The high primary productivity characterizing estuarine systems, in combination with their deep-water circulation, favor the accumulation of respiratory CO_2 at depth in stratified estuaries and a further decrease in pH (Taguchi et al. 2010; Cai et al. 2011; Mucci et al. 2011, Wallace et al. 2014; Hagens et al. 2015). In urbanized areas, this phenomenon can be exacerbated by eutrophication (Borges and Gypens 2010; Sunda and Cai 2012; Melzner et al. 2013). Since variations in pH in coastal waters are typically recurrent and of greater amplitude than those observed in the open ocean, one could surmise that the estuarine biota will be more resilient to pH fluctuations than open ocean biota. In order to evaluate the risk posed by ocean acidification on marine organisms in coastal systems, it is thus essential to know the chemical properties of source waters, the relative contribution of each to the coastal waters and their temporal variations. This knowledge is also required in order to develop realistic experimental protocols to assess the sensitivity of estuarine organisms to ocean acidification.

The head of the Laurentian Channel at the western limit of the Lower St. Lawrence Estuary (LSLE, Figure 1) is one of the most dynamic regions of the St. Lawrence Estuary. Here, complex tidal phenomena due to rapid shoaling (tidal movements, including internal tides and strong flows over the steep entrance sill) generate significant mixing of near-surface waters with the deeper saline waters, resulting in a nutrient-rich surface layer that sustains the feeding habitat of several large marine mammals. Four different water masses converge at this location: the brackish surface waters of the Upper St. Lawrence Estuary (USLE), the brackish surface waters discharged at the mouth of the Saguenay Fjord, the cold intermediate layer (CIL) waters of the LSLE and the hypoxic bottom waters of the LSLE (Mucci et al. 2011). With the exception of the Saguenay River waters, the other water masses are supersaturated in CO_2 with respect to the atmosphere (Table 1), the supersaturation having been acquired from their tributaries and/or the accumulation of metabolic CO_2 from microbial respiration of autochtonous or allochthonous organic matter (Yang et al. 1996; Barth et al. 1999; Wang and Veizer 2000). The objective of this study was to assess how the confluence and mixing of these different water masses affect the chemical and biological properties of the surface waters over two tidal cycles at a fixed station at the head of the Laurentian Channel. After identifying the properties of the individual end-member water-mass types, we estimated the relative contribution of each water-mass type to the surface waters at the fixed station by solving for a set of linear equations for conservative and non-conservative properties. A reconstruction of the water column properties at the fixed station and a comparison with field measurements are used to identify factors that control the pH of surface waters in this region over the study period.

Study Site:

The St. Lawrence Estuary

The St. Lawrence Estuary (SLE) receives the second largest freshwater discharge (11900 m^3 s^{-1}) in North America (El-Sabh and Silverberg 1990). It begins at the landward limit of the salt intrusion near Ile d’Orléans and extends 400 km seaward to Pointe-des-Monts and the Gulf of St. Lawrence (GSL), a semi-enclosed sea connected to the Atlantic Ocean via Cabot Strait and the Strait of Belle-Isle (Fig. 1). The Upper St. Lawrence Estuary (USLE) is the relatively shallow, well mixed, and fully oxygenated transition zone between the mouth of the St. Lawrence River at Quebec City and the marine region ($S_P \approx 25$ and greater) beginning at Tadoussac (Fig. 1). At the transition between the Upper and Lower St. Lawrence Estuary, the water column deepens from 50 m to 300 m over less than 20 km, in an area characterized by diverse and complex tidal phenomena (Gratton et al. 1988; Saucier and Chassé 2000). The dominant bathymetric feature of the Lower St. Lawrence Estuary (LSLE) is the Laurentian Channel, a 1240 km long, 250-500 m deep submarine valley that extends from the edge of the eastern Canadian continental shelf, through Cabot Strait, to the confluence of the St. Lawrence Estuary and the Saguenay Fjord at Tadoussac. The water column in the LSLE is strongly stratified and, throughout most of the year, is characterized by three distinct layers (Dickie and Trites 1983): (1) a thin surface layer (25-50 m deep) of low salinity (27-32) flowing seaward, (2) an intermediate cold (-1 to 2°C) and saline (31.5-33) layer (CIL) that originates in the Gulf in the winter, extends to about 150 m depth, and flows landward, and (3) a warmer (4-6°C) and saltier (34-34.6) deep layer (150+ m) that flows landward (El-Sabh and Silverberg 1990). Two typical vertical profiles taken at one of our sampling stations, station 1B (Figure 1b: 48°19.8'N, 069°17.4'W; June 11, 2013; 16:48GMT) and at station 18 (Figure 1a: 49° 16.0, 064° 16.5; June 7, 2013; 16:01 GMT) are reproduced in Figure 2. The surface layer displays large seasonal variations in temperature and salinity due to atmospheric and buoyancy (i.e., runoff events) forcing. In winter, the surface layer becomes progressively colder and denser, as tributary flow decreases, air temperatures plummet, and ice forms, until it merges with the intermediate layer (Gilbert and Pettigrew 1997; Galbraith 2006). The deep waters are a mixture of Labrador Current and North Atlantic Central waters whose proportions vary on a decadal or secular timescale (Bugden 1991; Gilbert et al. 2005). The transit time of a parcel of water between the seaward end of the Laurentian Channel at the edge of the continental shelf and the head of the Channel at Tadoussac has been estimated at 4 to 7 years (Bugden 1991, Gilbert 2004) whereas the mean age of the deep waters of the LSLE is believed to be ~20 years (Mucci et al. 2011). Given the properties of the source waters, benthic and pelagic respiration along the Channel, and their mean age, the bottom waters of the LSLE are hypoxic (<20% oxygen saturation; Gilbert et al. 2005), charged with metabolic CO_2 and therefore acidified (Mucci et al. 2011). The landward end of the Laurentian Channel marks the transition from the Lower to the Upper St.

Lawrence Estuary, the mouth of the Saguenay Fjord, and the marine region ($S_P \approx 25$ and greater) beginning at Tadoussac (Fig. 1). Typical semi-diurnal (M2) tidal current amplitudes in the LSLE are on the order of 0.2 m s^{-1} (Saucier and Chassé 2000), so that tidal excursions are on the order of 3 km.

The Saguenay Fjord

The Saguenay Fjord is a 93 km long, 1-6 km wide and 275 m deep U-shaped submerged valley, bounded by sheer, vertical walls that reach up more than 300 m above the water line. Situated approximately 150 km northeast of Quebec City on the north shore of the St. Lawrence Estuary, it connects with the estuary at Tadoussac through a 20-m deep sill. Its bathymetry is defined by three basins separated by two sills at 60 and 120 m depth, located approximately 20 km and 30 km, respectively, from the mouth of the fjord. A short account of its geological history and physiographic features can be found in Schafer et al. (1990) and Locat and Levesque (2009).

The water column of the Saguenay Fjord is characterized by a sharp pycnocline that separates two distinct water masses. The thick bottom layer is well-mixed and oxygenated, with waters penetrating landward from the St. Lawrence Estuary as they episodically spill over the sills (Therriault and Lacroix 1977; Siebert et al. 1979; Stacey and Gratton 2001; Bélanger 2003; Belzile et al. 2015). Bottom-water salinities are approximately 30.5 (Mucci et al. 2000), with temperatures ranging from 0.4 to 1.7°C (Fortin and Pelletier 1995). The surface layer consists of brackish waters (S_P~0-10) resulting from the turbulent mixing of the outflow from the Saguenay River (and smaller tributaries such as the Valin, Ha! Ha! and Mars Rivers) and the underlying marine waters. The thickness of the surface layer, perhaps best defined by the depth of the 18.00 sigma-tee isopycnal, typically increases towards the mouth of the fjord, but pinches off towards the surface at high tide or when denser waters overspill the entrance sill. The surface water temperatures range from freezing in winter to 16°C in summer (Fortin and Pelletier 1995). Detailed hydrographic characteristics of the fjord can be found in Schafer et al. (1990) and Gratton et al. (1994).

Figure 3 shows a 3-day average of sea-surface temperatures derived from satellite data (OGSL 2014). A prominent tongue of cold surface waters due to upwelling and tidal mixing extends from the head of the Laurentian Channel (near Tadoussac) to about Rimouski. Our fixed station is located at the northern edge of this cold tongue.

Methods

Water column sampling

On June 10-15, 2013, we sampled the whole water column at six stations and surface waters (3 – 5 m below the surface) at four stations along a saw-tooth transect at the head of the Lower St. Lawrence Estuary (LSLE), the mouth of the Upper St. Lawrence Estuary (USLE) and the mouth of the Saguenay Fjord (Figure 1). In addition, we sampled the whole water column every four hours and surface waters (~3 m) every two hours over 50 hours at a fixed station (48°11.2'N, 69°34.4'W) a few kilometers east of the fjord's mouth in the northern half of the head of the LSLE in order to characterize changes in the properties of these surfaces waters over two tidal cycles. Finally, the whole water column at four stations (Stations 23, 22, 20, 18) in the LSLE and western Gulf of St. Lawrence was sampled on an earlier cruise (June 3-8, 2013) and these results served to better define the properties of the source-water types encountered at the fixed station (see *Water mass analysis* section below). Water samples were collected using a 12-Niskin bottle/CTD (SeaBird SBE 911) rosette sampler onboard the R/V Coriolis II. Sampling depths were typically, 3, 10, 20, 40, 60, 80, 100, 150 m deep, in addition to 15 m above the bottom. The pH (on the NBS scale - pH_{NBS}), dissolved oxygen (DO), temperature and conductivity probes were calibrated by the manufacturer during the winter months preceding the cruise. Nevertheless, discrete samples were taken from the Niskin bottles for laboratory measurements of pH (total proton concentration scale – pH_T), DO and salinity and the CTD records re-calibrated post-cruise. Additional surface water samples were collected, on distinct outings, in Chicoutimi (Saguenay River end-member) and near Quebec City (St. Lawrence River end-member) during or within a week of the research cruise.

Analytical methods

Discrete salinity samples taken throughout the water column were analyzed on a Guildline Autosal 8400 salinometer calibrated with IAPSO standard seawater. The instrument has a theoretical accuracy $< \pm 0.002$. Dissolved oxygen (DO) concentrations were determined by Winkler titration (Grasshoff et al. 1999) of water samples recovered from the Niskin bottles. The relative standard deviation, based on replicate analyses of samples recovered from the same Niskin bottle, was better than 1%. These measurements further served to calibrate the SBE-43 oxygen probe mounted on the rosette.

Water samples destined for pH and titration alkalinity (TA) measurements were transferred directly from the Niskin bottles to, respectively, 125 mL plastic bottles without headspace and 250 mL glass bottles, as soon as the rosette was secured onboard. In the latter case, a few crystals of $HgCl_2$ were added before the bottle was sealed with a ground-glass stopper and Apiezon® Type-M high-vacuum grease.

The pH of the 125 mL samples was determined onboard using a Hewlett-Packard UV-Visible diode array spectrophotometer (HP-8453A) and a 5-cm quartz cell after thermal equilibration of the sampling bottles in a constant temperature bath at 25.0±0.1°C. Phenol red (PR; Robert-Baldo et al. 1985) and *m*-cresol purple (mCP; Clayton and Byrne 1993) were used as indicators. The absorbance at the wavelengths of maximum absorbance of the protonated (HL) and deprotonated (L) indicators were measured and recorded. A similar procedure was carried out several times each day using TRIS buffers prepared at practical salinities (S_P) of ~35 and ~25 (Millero 1986). The pH on the total proton concentration scale (pH_T) of the samples and buffer solutions were calculated according the equation of Byrne (1987). The salinity-dependence of the dissociation constants and molar absorptivities of the indicators were taken from Robert-Baldo et al. (1985) for phenol red and from Clayton and Byrne (1993) for *m*-cresol purple. The salinity-dependence of the phenol red indicator dissociation constant and molar absorptivities was extended (from S_P = 5 to 35; Bellis 2002) to encompass the range of salinities encountered in this study, but computed pH_Ts from the revised fit were not significantly different from those obtained with the relationship provided by Robert-Baldo et al. (1985). All measurements were converted to the total proton scale using the salinity of each sample and the HSO_4^- association constants given by Dickson (1990). Reproducibility and accuracy of our TRIS buffer measurements were on the order of 0.005 pH units or better. The computed pH_Ts at 25°C and 1 atmosphere total pressure were then used in combination with the measured TA to calculate the pH_Ts at the in-situ temperature and pressure using the Microsoft Excel version of CO2SYS (Pierrot et al. 2006), based on the original algorithm of Lewis and Wallace (1998), and the carbonic acid dissociation constants of Cai and Wang (1998), the total boron concentration $[B]_T$ value from Uppström (1974), and the standard acidity constant of the HSO_4^- ion ($K(HSO_4)$) from Dickson (1990).

The titration alkalinity (TA) was determined at the land-based laboratory within one week of sampling by open-cell automated potentiometric titration (Titrilab 865, Radiometer®) with a pH combination electrode (pHC2001, Red Rod®) and a dilute (~0.025N) HCl titrant. The latter was calibrated against Certified Reference Materials (CRM Batch#94, provided by A. G. Dickson, Scripps Institute of Oceanography, La Jolla, USA). Samples were drawn from the 250 mL sample bottle and weighed on an analytical balance to ± 0.1 mg. The average relative error, based on the average relative standard deviation on replicate standard and sample analyses, was better than 0.15%.

Nutrients

Subsamples for nutrient determinations were filtered through a 0.45 µm disposable syringe filter to remove particles. Dissolved NH_4^+ concentrations were determined immediately onboard with the fluorometric method described by Holmes et al. (1999), with a detection limit of 0.01 µM. For nitrate, nitrite, soluble reactive phosphorus (SRP) and soluble reactive silicon (SRS), filtered samples were collected into acid-washed 15-ml polyethylene tubes and quickly frozen and stored at -20°C. Back at home laboratory, frozen samples were rapidly thawed and concentrations of inorganic nutrients were determined using the routine colorimetric method adapted from Hansen and Koroleff (2007) with a Bran and Luebbe Autoanalyzer III. The analytical detection limit was 0.02 µM for nitrite, 0.04 µM for nitrate+nitrite (hereafter dissolved inorganic nitrogen, DIN), 0.05 µM for SRP and 0.1 µM for silicate.

Isotopic composition

Water samples for isotopic analysis were collected in 13 mL screw-top plastic test tubes. The stable oxygen isotopic composition ($\delta^{18}O$) of the water samples was analyzed at the GEOTOP-UQAM stable isotope laboratory. 200-µL aliquots of the water samples and two laboratory internal reference waters were transferred into 3-mL vials stoppered with a septum cap. The vials were then placed in a heated rack maintained at 40°C. Commercially available CO_2 gas was introduced in all the vials using a Micromass AquaPrep and allowed to equilibrate for 7 hours. The headspace CO_2 was then sampled by the Micromass AquaPrep, dried on a -80°C water trap, and analyzed on a Micromass Isoprime universal triple collector isotope ratio mass spectrometer in dual inlet mode. Data were normalized against the two internal reference waters, both calibrated against V-SMOW and V-SLAP. Data are expressed in ‰ with respect to V-SMOW, and the average relative standard deviation on replicate measurements of sample waters is better than 0.05‰.

Water mass analysis

The water mass analysis was performed using the optimum multi-parameter algorithm (OMP) of Karsteen and Tomczak (1999), originally developed by Tomczak (1981). OMP analysis is based on a simple model of linear mixing. It assumes that all water mass properties undergo the same mixing process, i.e. their mixing coefficients are identical, as is the case in turbulent mixing. The spatial water mass distribution can therefore be determined through a linear set of mixing equations. OMP determines the contributions of pre-defined end-member water masses (so called source-water types or SWT) to a sample. The SWT contributions or fractions (X_i) for each data point are obtained by finding the best linear mixing combination in parameter space defined by temperature, salinity, oxygen, total alkalinity and $\delta^{18}O$ which minimizes the residuals in a non-negative least squares analysis. The solution includes two physically realistic constraints: (i) the contributions from all sources must add up to 100%, and (ii) all contributions have to be non-negative.

Based on the description of the water circulation in the LSLE, four different source-water types contribute to the water column properties at the head of the Laurentian Channel: the freshwaters of the St. Lawrence and Saguenay Rivers, the saline and cold intermediate layer water and the upwelling saline hypoxic bottom water of the LSLE. Even though the properties of the source-water types are variable in both space and time, we use the dataset acquired during this study as well as data acquired a week before on another cruise along a seaward transect through the Lower Estuary and Gulf of St. Lawrence to define the most representative properties for each source-water type (Table 1). This allows the direct comparison of the water mass fractions and their vertical distribution at the time of sampling. Whereas OMP analysis was initially used to distinguish and calculate the relative contributions of each source-water type in a parcel of water using temperature, practical salinity (S_P) and nutrient data (Mackas et al. 1987), in this study, we used S_P, the titration alkalinity (TA), and $\delta^{18}O(H_2O)$ as conservative tracers as well as temperature and dissolved O_2 (DO) concentrations as non-conservative tracers, to constrain the water mass analysis. Non-conservative tracers should be applied with caution in OMP, because of temporal and spatial variability, particularly in the surface waters. For example, the temperature of the Saguenay River water ranges from 0°C in winter to +16°C in summer whereas the temperature of the St. Lawrence River ranges from 0°C in winter to >20°C in summer. Dissolved O_2 concentration was also used as a non-conservative tracer, because it is a function of temperature (e.g. O_2 solubility increases with decreasing temperature and salinity) and, like ΣSi and SRP, also a function of primary production and biological respiration. Consequently, end-member matrix and sample observations were multiplied by a diagonal weight matrix to account for differences in tracer reliability, environmental variability, and precision of the data (Table 2). The error associated with the water mass fraction analysis was estimated to be about ±10% of the fractional values (Macdonald et al. 1989; Lansard et al. 2012).

Results and discussion

Variations of the water properties over two tidal cycles

Figures 4a-l show time-series of water property profiles from the CTD (1-m resolution) at the fixed station (SF) over two tidal cycles from June 13 to June 15, 2013. Results of the OMP analysis are presented in Figures 5a-d.

The tides are very strong in the fixed station region. The impact of tides on the local circulation is described in detail in Saucier and Chassé (2000). Near the SF, the tidal elevation in the channel can be larger than 5 m (unpublished data) at the spring tide. Mertz and Gratton (1990) reported internal oscillations on the order of 40-60 m over a tidal semi-diurnal cycle. Similar oscillations can be observed on Figures 4a,b,c. The cold, upwelled water can reach the surface and be observed flowing downstream as on Figure 3. As observed on this figure, our SF is located at the edge of these cold surface waters.

Surface salinities decrease and temperatures increase during ebb tide (Figs. 4a,b), as freshwaters from the Saguenay and the St. Lawrence Rivers, but mostly of the latter (Figs. 5a,b), intrude into the Lower St. Lawrence Estuary (LSLE) and at our fixed station. The intrusion is detectable to depths of about 30 m and accompanied by a slight (less than 0.1 pH unit) decrease in pH (Fig. 4f). Higher salinity, lower temperature and higher pH waters impinge closer to the surface during the flood tide whereas patches of low pH waters from the Saguenay Fjord persist at the surface well into flood tide (Figs. 4a,b,f). The former correspond to the upwelling/invasion of the cold intermediate layer (CIL) nearly up to the surface where it accounts for more than 80% of the mixture (Fig. 5c). Temporal variations of the surface-water titration alkalinity (TA) and dissolved inorganic carbon (DIC) concentrations are almost perfectly correlated with those of the salinity (Figs. 4e,g). Temporal variations of the surface-water major nutrient concentrations are more diffuse, but are nonetheless either correlated (SRP ($r^2 = 0.63$); Fig. S1) or anti-correlated (DIN ($r^2 = 0.46$) and ΣSi ($r^2 = 0.62$); Fig. S1) to salinity in the top 3 m, reflecting the differential input from the freshwaters (Saguenay and St. Lawrence Rivers) and the CIL.

Irrespective of the tide, dissolved oxygen concentrations remain high (> 260 µM, Fig. 4d) throughout the top 80-100 m of the water column. Likewise, the computed pCO_2 in the top 80 m of the water column is slightly supersaturated with respect to the atmosphere (~ 400 µatm) and shows few discernible features, except for a greater pCO_2 supersaturation at low tide when the contribution of freshwaters from the St. Lawrence River and Saguenay Fjord, both of which are rich in metabolic CO_2 and dissolved silicate (as well as ammonium in the latter case) relative to the CIL, are maximum (Fig. 5a,b).

As expected, below 150 m depth, hypoxic bottom waters are dominated by Atlantic waters that enter the Gulf and Estuary through Cabot Strait. These waters intrude to depths as shallow as 80 m at high tide (Fig. 5d).

pH in the surface waters

The pH_T of the surface waters (top 3 m) varied from 7.855 to 7.934 during the 50-hour survey, nearly as much as the world's oceans have experienced as a result anthropogenic CO_2 uptake over the last century (Caldeira and Wickett 2005). The pH_T of surface waters is determined by the relative contribution of the three source-water types (SLW, SRW, and CIL), itself determined in great part by tidal mixing, as well as by gas exchange with the atmosphere, the addition of metabolic CO_2 through bacterial respiration and biological uptake of CO_2 through photosynthesis. Mucci et al. (2011) reported on the variation of surface-water (0-16 m depth interval) pH over the period 1933-2009 (also limited to the ice-free season) in the Lower St. Lawrence Estuary (LSLE). Unlike the deeper waters that have become hypoxic and acidified, the pH of surface waters shows no systematic variations over this period. Although the intra-annual variability reaches ~0.1 pH unit, the inter-annual variability is nearly null (slope = 0, $p > 0.05$; i.e., no statistically significant temporal variation). Along the Estuary and Laurentian Channel, pH variations can exceed the intra-annual variability in the LSLE as the salinity and balance between respiration and photosynthetic rates vary (Dinauer and Mucci 2017).

Throughout the three-day survey, waters in the surface layer (0-3 m) at the sampling sites were always supersaturated in CO_2 (443-550 μatm) with respect to the atmosphere at the time of sampling. The saturation state of the surface mixed layer water with respect to aragonite, given by:

$$\Omega_A = [Ca^{2+}][CO_3^{2-}]/K^*_A \qquad (1)$$

where K^*_A is the stoichiometric solubility of aragonite at the in-situ temperature and salinity and 1 atmosphere total pressure (Mucci, 1983), varied little during the sampling period and was close to saturation (Ω_A = 0.88 to 1.02, 0.95 ± 0.03, n=27, Fig. 6), but fell slightly below saturation (as low as Ω_A = 0.88) at low tide. Given the ratio of the stoichiometric solubility constants (K^*_A/K^*_C

= 1.5; Mucci, 1983), the saturation state of the surface waters with respect to calcite was close to 1.5. Deeper waters became undersaturated with respect to aragonite below 60-80 m reaching saturations as low as 0.70, but remained supersaturated with respect to calcite to the bottom at the fixed station.

Validation of the OMP analysis

Using the results of the OMP analysis and the source-water type properties in Table 1, the total alkalinity (TA), DIC and nutrient concentrations of each discrete water sample at the fixed station was calculated, over the whole time series, assuming conservative mixing (i.e., closed system). These computed values were then used as input parameters into CO2SYS to calculate the pH_T of the mixture and results compared to measured values. Differences between the calculated and observed surface waters properties are compiled in Table 3; these reflect changes to the water properties beyond those that can be accounted for by mixing of the source waters. The ΔpHcalc-meas values (thereafter referred to as ΔpH_T) of the surface waters (1-3 m) are all negative (-0.004 to -0.066), indicating that either CO_2 was lost by ventilation to the atmosphere or taken up by photosynthesis during our observation period. As indicated above, surface waters remained supersaturated with respect to the atmosphere throughout the sampling period and thus served as a net source to the atmosphere. CO_2 exchange across the air-sea interface is, however, a slow process, much slower than for oxygen and most other gases (Zeebe and Wolf-Gladrow, 2001), particularly under the low wind conditions (~5-28 knots) experienced during the cruise. Given these wind speeds, the parameterizations of Raymond and Cole (2001) and Wanninkhof (2014) for the gas transfer velocity, an average surface water pCO_2 of 499 (± 26 μatm) during the sampling period, and a local atmospheric pCO_2 of 391 μatm, we estimated the air-sea CO_2 efflux (loss of CO_2 to the atmosphere) to range between 2.6 and 4.8 mmol m^{-2} d^{-1}. Over our sampling period, the loss of CO_2 to the atmosphere did not affect the DIC budget significantly (less than 1 μmol/kg) and would have increased the surface-water pH by at most 0.003 unit, slightly below the uncertainty of our field measurements. The positive ΔpCO_2, ΔDIN and ΔSRP values (net DIC and nutrient uptake) as well as negative ΔDO values (net oxygen production) in the surface waters are clear evidence that photosynthesis (CO_2 uptake, pH increase) dominated over respiration (CO_2 production and pH decrease) and ventilation over the whole sampling period (Table 3). Unfortunately, in the absence of independent estimates of the absolute photosynthetic and/or respiration rates, we can only determine which of these two processes dominates. It is also interesting to note that, despite the large uncertainties in the model and the intrinsic patchiness of our measurements, the average ΔDIN:ΔSRP ratio (11 ± 4) nearly corresponds to the Redfield stoichiometry of 15-16 (Redfield et al. 1963) and the DIN: SRP ratio (12, $r^2 = 0.79$) below 30 m depth in the LSLE. When the surface-water ΔpH_T, ΔDIN, ΔSRP, ΔΣSi and ΔDO values are plotted as function of the time of the day, no systematic variation with daylight is apparent (Fig. 7). The study region is known to be an area of high primary productivity, notably during the spring tide periods when upwelling and internal waves amplitude are maximum (Therriault and Levasseur 1985, Levasseur and Therriault 1987), but can be strongly suppressed spring fresh-water runoff (Zakardjian et al. 2000). Hence, it is not surprising that we observe net autotrophy in the surface waters but our conservative mixing model is not able to resolve the diurnal cycle of photosynthesis and respiration, likely because it is not sensitive enough. Note that we have not modeled temporal variations of pH below the surface mixed layer (SML) because, as shown in Figure 5, below ~30m, the water column is entirely dominated by two water masses, the CIL between 30 and 50 m and

Atlantic (deep LSLE) waters below 150 m. In other words, with the exception of the SML, significant variations in water column composition in response to the tide are only found between 50 and 150 m. Given that these waters are isolated from the atmosphere (no gas exchange), below the euphotic zone (no photosynthesis), and respiration rates are negligible on the time scale of the experiments, temporal variations are simply due to tidal oscillations.

Susceptibility of estuarine waters to acidification resulting from direct anthropogenic CO_2 uptake

As noted above, most inner (river-dominated) estuaries are net sources of CO_2 to the atmosphere (Cai and Wang 1998; Chen and Borges 2009; Regnier et al. 2013). Their elevated DIC enrichments and pCO_2 supersaturations can mainly be attributed to the *in situ* microbial degradation of internally and externally supplied organic carbon and the lateral transport of inorganic carbon from rivers, coastal wetlands and ground waters (Bauer et al., 2013). Thus, these waters do not directly take up anthropogenic CO_2 from the atmosphere. Nonetheless, there have been several reports of weak CO_2 uptake by strongly stratified and/or marine-dominated (outer) estuaries (Koné et al. 2009; Maher and Eyre 2012; Cotovicz Jr. et al. 2015), including the Lower St. Lawrence Estuary (Dinauer and Mucci 2017). The resistance of these estuarine waters to a decrease in pH in response to CO_2 uptake is equated to a multiple of the carbonate ion concentration ($[CO_3^{2-}]$) (Stumm and Morgan 1996), and the latter, within the pH range of most of these ($7.5 < pH_T < 8.1$), is approximated by TA – DIC (Broecker and Peng 1982).

Variations of the saturation state of waters with respect to aragonite (or calcite) depend on the calcium and carbonate ion concentration product and the mineral solubility under in-situ conditions (Eqn. 1). The $[Ca^{2+}]$ in estuarine waters is determined by the composition and mixing ratio of the freshwater and seawater end-members, but given its high and conservative concentration in seawater, the freshwater signature typically becomes indistinguishable (within a 1% deviation of the diluted seawater value) from that of seawater above a salinity of ~14. The minimum salinity measured during our survey was 24.82. Hence, the $[Ca^{2+}]$ can accurately be estimated from the measured salinities, i.e., $[Ca^{2+}] = S_P * 0.01028/35$ (Millero 2013). Both $[Ca^{2+}]$ and K^*_A increase with salinity and to a similar extent (31% and 32.5%, respectively, over the range of salinities encountered during our study), so that Ω_A varies almost exactly with the $[CO_3^{2-}]$. Hence, again, the impact of CO_2 uptake on the saturation state of most marine-dominated estuaries is almost exclusively related to changes in $[CO_3^{2-}]$ which, as noted above, can be approximated by (TA – DIC).

Biological response of some local $CaCO_3$-secreting invertebrates to ocean acidification

Atmospheric CO_2 uptake lowers the pH, the carbonate ion concentration and saturation state of natural waters with respect to calcite and aragonite (Ω_C and Ω_A, respectively). Consequently, the ability of many organisms to calcify is reduced by a decrease in the saturation state of the waters and sediments they inhabit (Gazeau et al. 2013; Clements and Hunt 2017). Aragonite being 50% more soluble than calcite (Mucci, 1981), organisms whose shells or skeletons are partially or wholly aragonitic will be more susceptible to acidification.

Aragonite-undersaturated waters ($\Omega_A < 1$) dominate the top 20 metres of the water column at the head of the Laurentian Channel except when the CIL intrudes almost up to the surface at high tide. Below the CIL, the aragonite saturation depth ($\Omega_A = 1$) oscillates between 40 and 90 m reaching the shallowest depths at high tide when these waters are brought closer to the surface. Hence, the recruitment, growth, metabolism and survival of calcifying invertebrates and other benthic organisms exposed to these waters could be deleteriously affected (Parker et al. 2012; Gazeau et al. 2010; Talmage et al. 2010; Kuhihara 2008).

Commercial harvesting of bivalve shellfish (scallops, soft-shell clams, mussels, Atlantic surf-clams, Atlantic razor clams), echinoids (green sea urchin), and gastropods (common whelk) in Quebec sustains several coastal communities with annual landings in the range of 2.5-4 million dollars (DFO; http://www.qc.dfo-mpo.gc.ca/peches-fisheries/recreative-recreational/mollusque-mollusc-eng.asp?p=/peches-fisheries/recreative-recreational/mollusque-mollusc-eng.html). Scallops (e.g., *Chlamys islandica*), soft-shell clams (e.g., *Mya arenaria*), the common whelk (e.g., *Buccinum undatum*) and the green sea urchin (e.g., *Stronylocentrotus droebachiensis*) are found on the seafloor near the head of the Laurentian Channel and, with the exception of scallops (Hutin et al. 2005), are mostly harvested from no more than 20 m depth (Bernard Saint-Marie, DFO, pers. comm.). Except for the green sea urchin, harvesting of the other species has declined steadily since the beginning of the new millennium and there are currently no active commercial shellfish fisheries in this region while recreational harvesting of scallops is now forbidden. The shells of most bivalves and whelks found in the study area are composed of a combination of calcite and aragonite (micro-) structural components (groups and layers) whereas the body and spines of sea urchins are typically composed of high-magnesium calcite (more soluble than aragonite) and, thus, their constant exposure to the aragonite-undersaturated (corrosive) waters in the top 20 m of the water column and along the shorelines in the vicinity of the study area could possibly have contributed, along with overfishing (Archambault and Goudreau 2006), to their decline. Since the habitat of scallops extends to depths of 80 meters (the largest scallop bed in the vicinity of Tadoussac is situated 5-10 km downstream of Ile Rouge in 40-80 m of water; Hutin et al. 2005), this would put them well into the aragonite-undersaturated (corrosive) waters found below the CIL.

To our knowledge, no specific study of the impacts of elevated pCO_2s (lower pH and Ω_A) has been carried out on *Chlamys islandica* and *Buccinum undatum*, but studies conducted on other species of scallops and whelk have reported deleterious effects on calcification and growth of the former and the nutritional properties of the latter (Tate et al. 2017; Andersen et al. 2013). Conversely, in addition to lowered calcification rates, the impacts of elevated pCO_2 on *Mya arenaria* were found to extend to their burrowing behavior, post-settlement dispersal (Clements et al. 2016) as well as predator-prey interactions (Glaspie et al. 2017) whereas, in the case of *Stronylocentrotus droebachiensis*, the effects extend to the fecundity, gonad growth, feeding rates and susceptibility to metal toxicity (Lewis et al. 2016; Dupont et al. 2013; Siikavuopio et al. 2007).

Notwithstanding the potential impact of ocean acidification (OA) on the organisms listed above, one should consider that these organisms may have, over time, developed a tolerance or acclimatized to the high-amplitude and high-frequency (diurnal, seasonal) variations of environmental variables (T, S, pH) encountered in dynamic estuaries such as the USLE, as has been demonstrated in long-term exposures to elevated pCO_2 (Dupont et al. 2013; Moulin et al. 2015; Uthicke et al. 2016). Whereas the above discussion is limited to commercially-harvested $CaCO_3$-secreting benthic organisms, OA may impact on the metabolic activity (e.g., survival, growth, reproduction) of many other organisms, but an expanded discussion of these would be well beyond the scope of this paper given the range of responses documented in the literature (e.g., Doney et al. 2009).

In summary, the pH of surface waters at the head of the Laurentian Channel is modulated by tides and mixing of three source–water types, the relatively high alkalinity (TA) and dissolved inorganic carbon (DIC)-rich water of the St. Lawrence River (TA-DIC <0), the TA and DIC-poor water of the Saguenay River (TA-DIC) <0) and saline waters of the TA and DIC-rich cold intermediate layer (CIL) of the St. Lawrence Estuary (TA-DIC) >0) that upwell in this region. Consequently, in-situ pH_T values lower than 8.0 are found below the CIL or 80 m depth and in the top 30 m of the water column. Nevertheless, upwelling of the TA-rich CIL and mixing with lower salinity waters near the surface limit pH excursions within a narrow range (7.86 to 7.93) as the (TA-DIC) of the mixture at our study site (head of the Laurentian Channel) was always positive. The presence of the CIL also appears to impede the upwelling of the hypoxic, CO_2-rich and aragonite-undersaturated bottom waters of the Lower St. Lawrence Estuary (LSLE) to depths shallower than about 80 m (Figure 5), although the large density gradient, as well as the tidal (~5 m) and internal-wave amplitudes (maximum 50-60 m), would not allow bottom waters to intrude at the surface. The CIL is not unique to the SLE as similar layers are common in other subpolar basins (Osafune and Yasuda 2006; Cyr et al. 2015). Organisms living within the first 20 meters of the water column at the head of the Laurentian Channel are bathed, at low tide, by aragonite-undersaturated waters ($\Omega_A < 1$) intruding from the St. Lawrence and Saguenay Rivers. Likewise, those that live below 80 meters depth, below the CIL, such as the largest scallop bed in the area, are continuously exposed to the aragonite-undersaturated bottom waters ($\Omega_A < 1$) of the LSLE that upwell up to nearly 40 metres from the surface at high tide. Whereas the growth, recruitment, and other metabolic functions of $CaCO_3$-secreting invertebrates exposed to these aragonite-undersaturated waters may be deleteriously affected, some of these organisms may have, over time, developed a tolerance or acclimatized to the high-amplitude and high-frequency (diurnal, seasonal) variations of environmental variables (T, S, pH) encountered in this dynamic environment.

Acknowledgements-

We wish to thank the Captain and crew of the Coriolis II for their help during a trying research cruise. We also wish to acknowledge the help of Gilles Desmeules and Sylvain Blondeau for their dedicated electronic and field sampling support as well as Dr. Michel Starr, Qiang Chen, Liliane St-Amand, Sonia Michaud, Hourssem Gaalloul, Jory Cabrol, Robin Bénard, Honghai Zhang for their help in field data acquisition. Most of the plots in this study were created with the ODV Software [Schlitzer, 2009]. This research was funded by a Team grant from the Fonds Québécois de recherche nature et technologies (FQRNT-Équipe-165335) and a Ship-Time Allocation grant from the Natural Sciences and Engineering Research Council of Canada (NSERC-STAC-436804-2013). Finally, we would like to thank the journal reviewers for their constructive comments.

References

Andersen, S., Grefsrud, E.S. and Harboe, T. 2013. Effect of increased $p\mathrm{CO}_2$ levels on early shell development in great scallop (*Pectin maximus* Lamarck) larvae. Biogeosci. 10: 6161-6184.

Archambault, P., and Goudreau, P. 2006. Effect of the commercial fishery on the Ile Rouge Iceland scallop (*Chlamys islandica*) bed in the St. Lawrence estuary: assessment of the impacts on scallops and the benthic community. DFO Can. Sci. Advis. Sec. Res. Doc. 2006/079.

Barth, J.A.C., and Veizer, J. 1999. Carbon cycle in St Lawrence aquatic ecosystems at Cornwall (Ontario), Canada: seasonal and spatial variations. Chem. Geol. **159:** 107–128.

Barwell-Clarke, J,, and Whitney, F. 1996. Institute of Ocean Sciences Nutrient Methods and Analysis. Can. Tech. Rep. Hydrogr. Ocean Sci. 182: vi + 43 p.

Bauer, J.E., Cai, W.-J., Raymond, P.A., Bianchi, T.S., Hopkinson, C.S., and Regnier, P.A. 2013. The changing carbon cycle of the coastal ocean, Nature **504:** 61–70.

Bélanger, C. 2003. Observation and Modelling of a Renewal Event in the Saguenay Fjord. Ph.D. thesis, Institut des Sciences de la Mer de Rimouski, Université du Québec à Rimouski, Rimouski, QC, 235 pp.

Bellis, A. 2002. Spectrophotometric determination of pH in estuarine waters using Phenol Red. B.Sc. Thesis, Department of Earth and Planetary Sciences, McGill University, 53pp.

Belzile, M., Galbraith, P.S., and Bourgault, D. 2015. Water renewals in the Saguenay Fjord. J. Geophys. Res. Oceans **120:** 1-20 doi:10.1002/2015JC011085

Broecker, W.M., and Peng, T-H. 1982. *Tracers in the Sea*, Eldigio Press, Palisades, NY, 690 pp.

Bugden, G.L. 1991. Changes in the temperature-salinity characteristics of the deeper waters of the Gulf of St. Lawrence over the past several decades. *In* The Gulf of St. Lawrence: Small Ocean or Big Estuary? *Edited by* J.-C. Therriault, Can. Spec. Publ. Fish. Aquat. Sci. **113:** 139-147.

Byrne, R.H. 1987. Standardization of standard buffers by visible spectrometry. Anal. Chem. **59:** 1479-1481.

Cai, W.-J., and Wang, Y. 1998. The chemistry, fluxes, and sources of carbon dioxide in the estuarine waters of the Satiala and Altamaha Rivers, Georgia. Limnol. Oceanogr. **43:** 657-668.

Cai, W.-J., Hu, X., Huang, W.-J., Murrell, M. C., Lehrter, J. C., Lohrenz, S. E., Chou, W.-C., Zhai, W., Hollibaugh, J. T., Wang, Y. , Zhao, P., Guo, X. , Gundersen, K., Dai, M., and Gong, G.-C. 2011. Acidification of subsurface coastal waters enhanced by eutrophication. Nature Geosci. **4**, 766–770.

Caldeira, K., and Wickett, M.E. 2005. Ocean model predictions of chemistry changes from carbon dioxide emissions to the atmosphere and ocean. J. Geophys. Res.-Oceans **110:** C09S04, doi:10.1029/2004JC002671.

Chen, C.-T. A., and Borges, A.V. 2009. Reconciling opposing views on carbon cycling in the coastal ocean: Continental shelves as sinks and near-shore ecosystems as sources of atmospheric CO_2. Deep-Sea Res. II **56:** 578-590.

Clayton, T.D., and Byrne, R.H. 1993. Spectrophotometric seawater pH measurements: total hydrogen ion concentration scale calibration of m-cresol purple and at-sea results. Deep-Sea Res. **40:** 2115–2129.

Clements, J.C., and Hunt, H.L. 2017. Effects of CO2-driven sediment acidification on infaunal marine bivalves: A synthesis. Mar. Poll. Bull. **117:** 6-16.

Cotovicz Jr., L. C., Knoppers, B. A., Brandini, N., Costa Santos, S. J., and Abril, G. 2015. A strong CO_2 sink enhanced by eutrophication in a tropical coastal embayment (Guanabara Bay, Rio de Janeiro, Brazil), Biogeosciences **12:** 6125–6146

Cyr, F., Bourgault, D., and Galbraith, P.S. 2015. Behavior and mixing of a cold intermediate layer near a sloping boundary. Ocean Dynamics **65:** 357-374.

Dickie, L., and Trites, R.W. 1983. The Gulf of St. Lawrence. *In* Estuaries and Semi-enclosed Seas, *Edited by* L. Dickie and R.W. Trites, Elsevier Scientific Publication, Amsterdam, pp. 403-425.

Doney, S.C., Balch, W.M., Fabry, V.J., and Feely, R.A. 2009. Ocean acidification: A critical emerging problem for ocean sciences. Oceanogr. **22:** 16-25.

Dickson, A.G. 1990. Standard potential of the ($AgCl + 1/2H_2 = Ag + HCl_{(aq)}$) cell and the dissociation constant of bisulfate ion in synthetic sea water from 273.15 to 318.15 K. J. Chem. Thermodyn. **22:** 113-127.

Dinauer, A., and Mucci, A., 2017. Spatial variability of surface-water pCO_2 and gas exchange in the world's largest semi-enclosed estuarine system: St. Lawrence Estuary (Canada). Biogeosciences (in press).

Dupont, S., Dorey, N., Stumpp, M., Melzner, F., and Thorndyke, M. 2013. Long-term and trans-life-cycle effects of exposure to ocean acidification in the green sea urchin *Strongylocentrotus droebachiensis*. Mar. Biol. **160:** 1835-1843.

El-Sahb, M.I., and Silverberg, N. 1990. The St. Lawrence Estuary: introduction. *In* Oceanography of a Large-scale Estuarine System. *Edited by* M.I. El-Sabh and N. Silverberg, Springer-Verlag, New York, pp. 1-9.

Fabry, V.J., Seibel, B.A., Feely, R.A., and Orr, J.C. 2008. Impacts of ocean acidification on marine fauna and ecosystem processes. ICES journal of Mar. Sci. **65:** 414-432.

Feely, R. A., Alin, S.R., Newton, J., Sabine, C.L., Warner, M., Devol, A., Krembs, C., and Maloy, C. 2010. The combined effects of ocean acidification, mixing, and respiration on pH and carbonate saturation in an urbanized estuary. Estuar. Coast. Shelf Sci. **88:** 442−449.

Fortin, G.R., and Pelletier, M. 1995. Synthèse des connaissances sur les aspects physiques et chimiques de l'eau et des sédiments du Saguenay. Environnement Canada Technical Report., Conservation de l'environnement, Centre Saint-Laurent, Montreal, QC

Frankignoulle, M., Bourge, I., and Wollast, R. 1996. Atmospheric CO_2 fluxes in a highly polluted estuary (The Scheldt). Limnol. Oceanogr. **41:** 365–369.

Frankignoulle, M., Abril, G., Borges, A., Bourge, I., Canon, C., Delille, B., Libert, E., and Théate, J.M. 1998. Carbon dioxide emission from European estuaries. Science **282:** 434–436.

Galbraith, P.S. 2006. Winter water masses in the Gulf of St. Lawrence. J. Geophys. Res. Oceans **111:** C06022. doi: 10.1029/2005JC003159Gazeau, F., Gattuso, J.-P., Dawber, C., Pronker, A. E., Peene, F., Peene, J., Heip, C. H. R., and Middelburg, J. J. 2010. Effect of ocean acidification on the early life stages of the blue mussel *Mytilus edulis*, Biogeosciences, **7:** 2051–2060.

Gazeau, F., Parker, L.M., Comeau, S., Gattuso, J.-P., O'Connor, W.A., Martin, S., Pörtner, H.-O., and Ross, P.M., 2013. Impacts of ocean acidification on marine shelled molluscs. Mar. Biol. 160:2207–2245.

Gilbert, D. 2004. Propagation of temperature signals along the northwest Atlantic continental shelf edge and into the Laurentian Channel. *Abstract, ICES CIEM Annual Science Conference* September 22–25, Vigo, Spain.

Gilbert, D., and Pettigrew, B. 1997. Interannual variability (1948-1994) of the CIL core temperature in the Gulf of St. Lawrence. Can. J. Fish. Aquat. Sci. **54:** 57-67.

Gilbert, D., Gobeil, C., Sundby, B., Mucci, A., and Tremblay, G. 2005. A seventy-two year record of diminishing deep-water oxygen levels in the St. Lawrence estuary: the northwest Atlantic connection. Limnol. Oceanogr. **50:** 1654-1666.

Grasshoff, K., Kremling, K., and Ehrhardt, M. 1999. Methods of seawater analysis (3rd ed.). Wiley-VCH, Weinheim, Germany.

Gratton, Y., Mertz, G., and Gagné, J.A. 1988. Satellite observations of tidal upwelling and mixing in the St. Lawrence Estuary. J. Geophys. Res. **93:** 6947-6954.

Gratton, Y., Lefaivre D., and Couture, M. 1994. Océanographie physique du fjord du Saguenay. *In* Le fjord du Saguenay: Un Milieu Exceptionnel de Recherche. *Edited by* J.-M. Sévigny and C. M. Couillard, Ministère des Pêches et des Océans, Institut Maurice-Lamontagne, 8–16.

Hansen, H.P., and F. Koroleff F. 2007. Determination of nutrients. Methods of Seawater Analysis. Wiley-VCH Verlag GmbH. p. 159-228.

Holmes, R.M., A. Aminot, R. Kéroue, B.A. Hooker, and B.J. Peterson. 1999. A simple and precise method for measuring ammonium in marine and freshwater ecosystems. Canadian Journal of Fisheries and Aquatic Sciences **56(10):**1801-1808.

Hutin E., Y. Simard, and P. Archambault. 2005. Acoustic detection of a scallop bed from a single-beam echosounder in the St. Lawrence. ICES J. Mar. Sci. **62:** 966-983.

Intergovernmental Panel on Climate Change. 2007. Summary for Policymakers. *In* Climate Change 2007: The Physical Sciences Basis. Working Group I Contribution to the Fourth Assessment Report of the IPCC, *Edited by* S. Solomon, S. et al., Cambridge Univ. Press, Cambridge.

Karsteen, J. and M. Tomczak, 1999. OMP Analysis Package for Matlab, Version 2.0, Available from http://omp.geomar.de/.

Koné, Y. J. M., Abril, G., Kouadio, K. N., Delille, B., and Borges, A. V. 2009. Seasonal variability of carbon dioxide in the rivers and lagoons of Ivory Coast (West Africa), Estuaries and Coasts, **32:** 246–260.

Kroeker, K.J., Kordas, R.L., Crim, R., Hendriks, E., Ramajo, L., Singh, G.D., Duarte, C.M., and Gattuso, J.-P. 2013. Impacts of ocean acidification on marine organisms: quantifying sensitivities and interaction with warming. Global Change Biol. 19: 1888-1896.

Kurihara, H. 2008. Effects of CO_2-driven ocean acidification on the early developmental stages of invertebrates, Mar. Ecol.-Prog. Ser., **373:** 275–284.

Lansard, B., Mucci, A., Miller, L.A., Macdonald, R.W., and Gratton, Y. 2012. Seasonal variability of water mass distribution in the southeastern Beaufort Sea determined by total alkalinity and $\delta^{18}O$. J. Geophys. Res.-Oceans **117:** C03003, 19 pp.

Levasseur, M., and Therriault, J.-C. 1987. Phytoplankton biomass and nutrient dynamics in a tidally induced upwelling: the role of the NO_3:SiO_4 ratio. Mar. Ecol. Prog. Ser. **39:** 87-97

Lewis, E., and Wallace, D.W.R. 1998. Program Developed for CO_2 System Calculations. ORNL/CDIAC-105. Carbon dioxide Information Analysis center, Oak Ridge National Laboratory, US Department of Energy, Oak Ridge, TN. Available from http://cdiac.esd.ornl.gov/oceans/co2rprt.html.

Locat, J., and Levesque, C. 2009. Le Fjord du Saguenay: Une physiographie et un registre exceptionnels. Revue des Sciences de l'Eau **22:** 135-157.

Maher, D. T., and Eyre, B. D. 2012. Carbon budgets for three autotrophic Australian estuaries: Implications for global estimates of the coastal air-water CO_2 flux, Global Biogeochem. Cycles **26:** GB1032, doi:10.1029/2011GB004075.

Macdonald, R.W., Carmack, E. C., McLaughlin, F., Iseki, A.K., Macdonald, D. M., and O'Brien, M.C. 1989. Composition and modification of water masses in the Mackenzie shelf estuary. J. Geophys. Res. **94:** 18057-18070

Mackas, D.L., Denman, K. L., and Bennett, A.F. 1987. Least squares multiple tracer analysis of water mass composition. J. Geophys. Res. **92:** 2907-2918.

Melzner, F., Thomsen, J., Koeve, W., Oschlies, A., Gutowska, M.A., Bange, H.W., Hansen, H.P., and Körtzinger, A. 2013. Future ocean acidification will be amplified by hypoxia in coastal habitats. Mar. Biol. **160:** 1875–1888.

Mertz, G., and Gratton, Y. 1990. Topographic waves and topographically induced motion in the St. Lawrence Estuary, *In* Oceanography of a Large-Scale Estuarine System: The St. Lawrence. M.I El-Sabh and N. Silverberg. vol. 39. New York, Springer-Verlag, pp. 94-108.

Meybeck, M. 1993. Riverine transport of atmospheric carbon: sources, global typology and budget, Water Air Soil Poll. **70:** 443–463.

Miller A. W., Reynolds, A.C., Sobrina, C., and Riedel, G.F. 2009. Shellfish face uncertain future in high CO_2 world: influence of acidification on oyster larvae calcification and growth in estuaries. PLoS ONE **4(5):** e5661, doi:10.1371/journal.pone.0005661.

Millero, F. J. 1986. The pH of estuarine waters. Limnol. Oceanogr. **34:** 839-847.

Millero, F.J. 2013. Chemical Oceanography, 4thEdition, CRC Press, Boca Raton, 469 pp.

Mucci, A. 1983. The solubility of calcite and aragonite in seawater at various salinities, temperatures and one atmosphere total pressure. Amer. Jour. Sci. **283:** 780-799.

Mucci, A., Richard, L.-F., Lucotte, M., and Guignard, C. 2000. The differential geochemical behavior of arsenic and phosphorus in the water column and sediments of the Saguenay Fjord Estuary, Canada. Aquat. Geochem. **6:** 293-324.

Mucci, A., Starr, M., Gilbert, D., and Sundby B. 2011. Acidification of Lower St. Lawrence Estuary bottom waters. Atmosphere-Ocean **49:** 206-213.

Observatoire Global du Saint-Laurent-OGSL, Available from http://ogsl.ca, (data downloaded on October 16, 2014).

Osafune, S., and Yasuda, I. 2006. Bidecadal variability in the intermediate waters of the northwestern subarctic Pacific and the Okhotsk Sea in relation to 18.6-year period nodal tidal cycle. J. Geophys. Res. **111:** C05007, 14 pp.

Parker, L. M., Ross, P. M., O'Connor, W. A., Borysko, L., Raftos, D. A., and Pörtner, H.-O. 2012. Adult exposure influences offspring response to ocean acidification in oysters, Glob. Change Biol., **18:** 82–92

Pierrot, D., E. Lewis, E., and D. Wallace, 2006. MS Excel Program Developed for CO_2 System Calculations. ORNL/CDIAC-105a, Carbon Dioxide Information Analysis Center, Oak Ridge National Laboratory, U.S. Department of Energy, Oak Ridge, Tennessee.

Raymond, P. A., and Cole, J. J. 2001. Gas exchange in rivers and estuaries: Choosing a gas transfer velocity. Estuaries and Coasts 24(2): 312–317.

Raymond P.A., Caraco, N.F., and Cole, J.J. 1997. Carbon dioxide concentration and atmospheric flux in the Hudson River. Estuaries **20:** 381–390.

Redfield A.C., Ketchum, B.H., and Richards, F. A. 1963. The influence of organisms on the composition of sea water, *In* The sea, Vol. 2, Edited by M. N. Hill, pp. 26–77. Wiley.

Regnier, P., Friedlingstein, P., Ciais, P., Mackenzie, F.T., Gruber, N., Janssens, I.A., Laruelle, G.G., Lauerwald, R., Luyssaert, S., Andersson, A.J., Arndt, S., Arnosti, C., Borges, A.V., Dale, A.W., Gallego-Sala, A., Goddéris, Y., Goossens, N., Hartmann, J., Heinze, C., Ilyina, T., Joss, F., LeRowe, D.E., Liefeld, J., Meysman, F.J.R., Munhoven, G., Raymond, P.A., Spahni, R., Suntharalingam, P., and Thullner, M. 2013. Anthropogenic perturbation of the carbon fluxes from land to ocean, Nat. Geosci., 6: 597–607

Ries, J. B., Cohen, A.L. and McCorkle, D.C. 2009. Marine calcifiers exhibit mixed responses to CO_2-induced ocean acidification. Geology **37:** 1131-1134.

Robert-Baldo, G., Morris, M.J., and Byrne, R.H. 1985. Spectrophotometric determination of seawater pH using phenol red. Anal. Chem. **57:** 2564-2567.

Sabine, C.L., Feely, R.A., Gruber, N., Key, R.M., Lee, K., Bullister, J.L., Wanninkof, R., Wong, C.S., Wallace, D.W.R., Tilbrook, B., Millero, F.J., Peng, T.-H., Kozyr, A., Ono, T., and Rios, A. 2004. The oceanic sink for anthropogenic CO_2. Science **305:** 367-371.

Saucier, F.J., and Chassé, J. 2000. Tidal circulation and buoyancy effects in the St. Lawrence Estuary. Atmosphere-Ocean **38:** 505-556.

Schafer, C.T., Smith, J.N., and Côté, R. 1990. The Saguenay Fjord: A major tributary to the St. Lawrence Estuary. *In* Oceanography of a Large-Scale Estuarine System: The St. Lawrence. M.I El-Sabh and N. Silverberg. vol. 39. New York, Springer-Verlag, pp. 378-420.

Schlitzer, R. 2009. Ocean Data View, http://odv.awi.de/, Alfred Wegener Inst. for Polar Mar. Res., Bremerhaven, Germany.

Siebert, G.H., Trites, R.W., and Reid, S.J. 1979. Deepwater exchange processes in the Saguenay Fjord. J. Fish. Res. Board Can. **36:** 42-53.

Stacey, M.W., and Gratton, Y. 2001. The energetics and tidally induced reverse renewal in a two-silled fjord. J. Phys. Oceanogr. **31:** 1599-1615.

Sunda W. G., and Cai, W.-J. 2012. Eutrophication induced CO_2-acidification of subsurface coastal waters: interactive effects of temperature, salinity, and atmospheric pCO_2. Environ. Sci. Technol. **46:** 10651–10659.

Stumm W., and Morgan J. J. 1996. *Aquatic Chemistry: Chemical Equilibria and Rates in Natural Waters*. 3rd ed., John Wiley & Sons, Inc., New York, NY, 780 pp.

Taguchi, F., and Fujiwara, T. 2010. Carbon dioxide stored and acidified low oxygen bottom waters in coastal seas, Japan. Estuar. Coast. Shelf Sci. **86:** 429−433.

Talmage, S. C. and Gobler, C. J.: Effects of past, present, and future ocean carbon dioxide concentrations on the growth and survival of larval shellfish, Proc. Natl. Acad. Sci. **107:** 17246–17251.

Tate, R.D., Benkendorff, K., Lah R.A., and Kelaher, B.P. 2017. Ocean acidification and warming impacts the nutritional properties of the predatory whelk, Dicathais orbita. J. Exp. Mar. Biol. Ecol. **493:** 7-13.

Therriault J.-C., and Lacroix, G. 1977. Penetration of the deep layer of the Saguenay Fjord by surface waters of the St-Lawrence Estuary. J. Fish. Res. Board Can. **112:** 77-96.

Therriault J.-C., and Levasseur, M. 1985. Control of phytoplankton production in the lower St. Lawrence estuary: Light and freshwater runoff. Nat. Can. **112:** 77-96.

Tomczak, M., 1981. A multiparameter extension of temperature/salinity diagram techniques for the analysis of non-isopycnal mixing. Prog. in Oceanogr. **10:**147-171.

Uppström, L.R. 1974.The boron/chlorinity ratio of deep-sea water from the Pacific Ocean. Deep Sea Research and Oceanographic Abstracts 21, 161-162.

Uthicke, S., Ebert, T., Liddy, M., Johansson, C., Fabricius, K.E., and Lamare, M. 2016. *Echinometra* sea urchins acclimatized to elevated pCO_2 at volcanic vents outperform those under present-day pCO_2 conditions. Global Change Biol. **22:** 2451-2461.

Wallace R.B., Baumann, H., Grear, J.S., Aller, R.C., and Gobler, C.J. 2014. Coastal ocean acidification: the other eutrophication problem. Estuar. Coast. Shelf Sci. **148**, 1–13.

Wang X., and Veiser, J. 2000 Respiration-photosynthyesis balance of terrestrial aquatic ecosystems, Ottawa area, Canada. Geochim. Cosmochim. Acta 64: 3775-3786.

Wanninkhof, R. 2014. Relationship between wind speed and gas exchange over the ocean revisited. Limnol. Oceanogr. Methods, 12(6): 351–362.

Yang C., Telmer, K.. and Veiser, J. 1996. Chemical dynamics of the “St. Lawrence” riverine system: δD_{H2O}, $\delta^{18}O_{H2O}$, $\delta^{13}C_{DIC}$, $\delta^{34}S_{sulfate}$, and dissolved $^{87}Sr/^{86}Sr$. Geochim. Cosmochim. Acta 60: 851-866.

Zakardjian B.A., Gratton Y. and Vézina A.F. 2000. Late spring phytoplankton bloom in the Lower St. Lawrence Estuary: the flushing hypothesis revisited. Mar. Ecol. Prog. Ser. 192: 31-48.

Zeebe, R.E., and Wolf-Gladrow, D. 2001. CO_2 in Seawater: Equilibrium, Kinetics, Isotopes, Amsterdam, Elsevier Science, Elsevier Oceanography Series, 346 pp.

Figure 1- a)

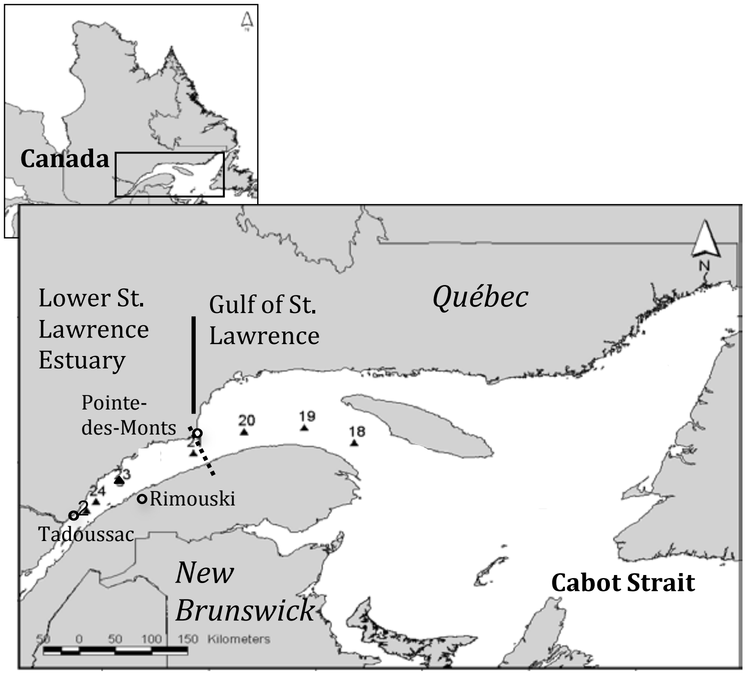

Figure 1- b)

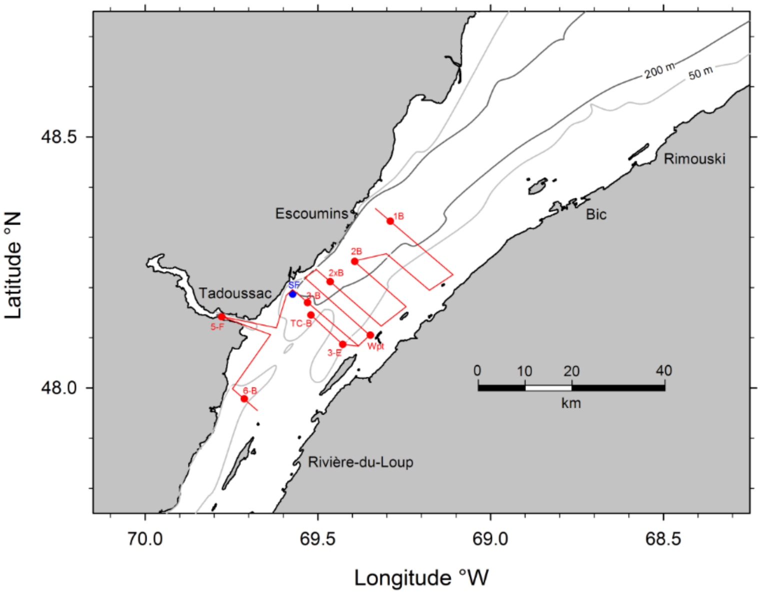

Figure 1. a) Map of the St. Lawrence Estuary and location of stations visited on a cruise immediately prior to this study (June 3-8, 2013) as well as b) the transect track and position of the fixed sampling station visited during this study (June 10-15, 2013). Water properties measured on the previous cruise and along the transect were used to define the water-type properties and served for the water mass analysis in OMP

Figure 2 –

a)

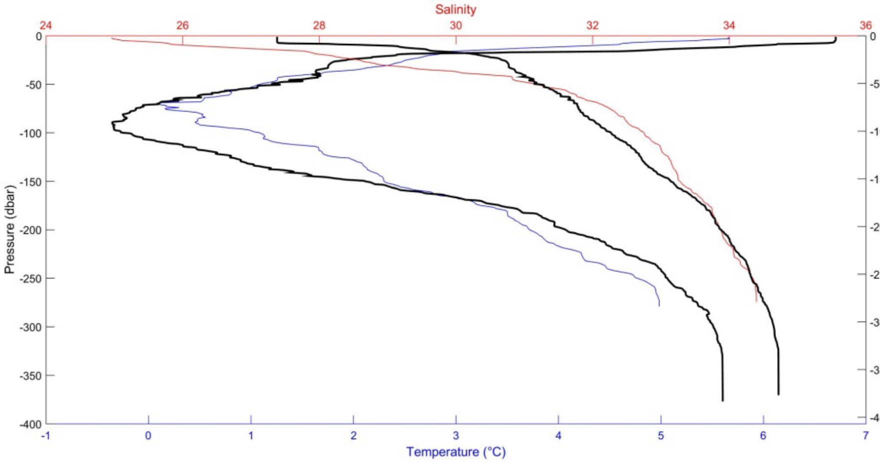

b)

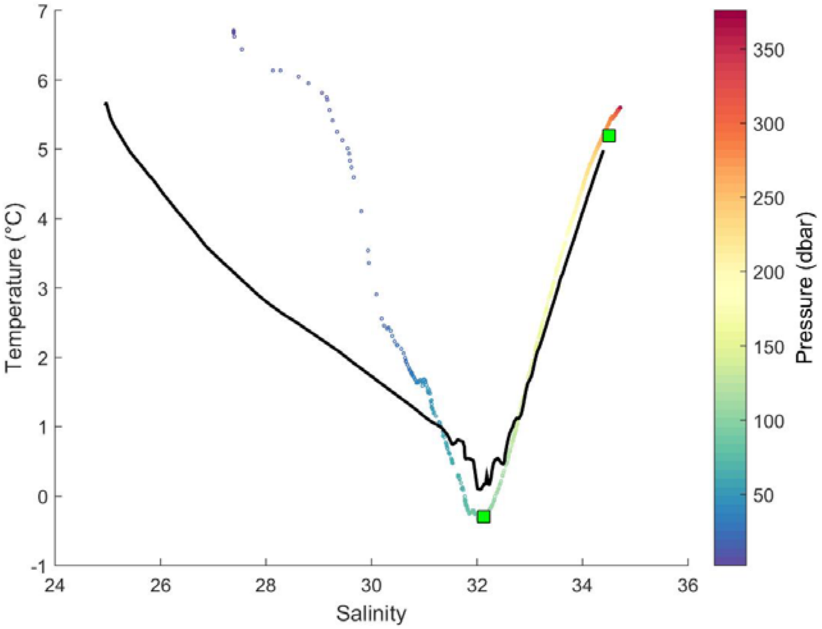

Figure 2. a) Vertical profiles of the salinity (red line) and temperature (blue line) throughout the water column as recorded at the fixed station on June 11, 2013 at 16:48 GMT. We also show the profiles (thick black lines) from station 18. The data are reproduced in a T-S diagram (b) that reflects the three-layer estuarine circulation in the Lower St. Lawrence Estuary. The green squares indicate the CIL and LSLE bottom-water endmembers.

Figure 3 -

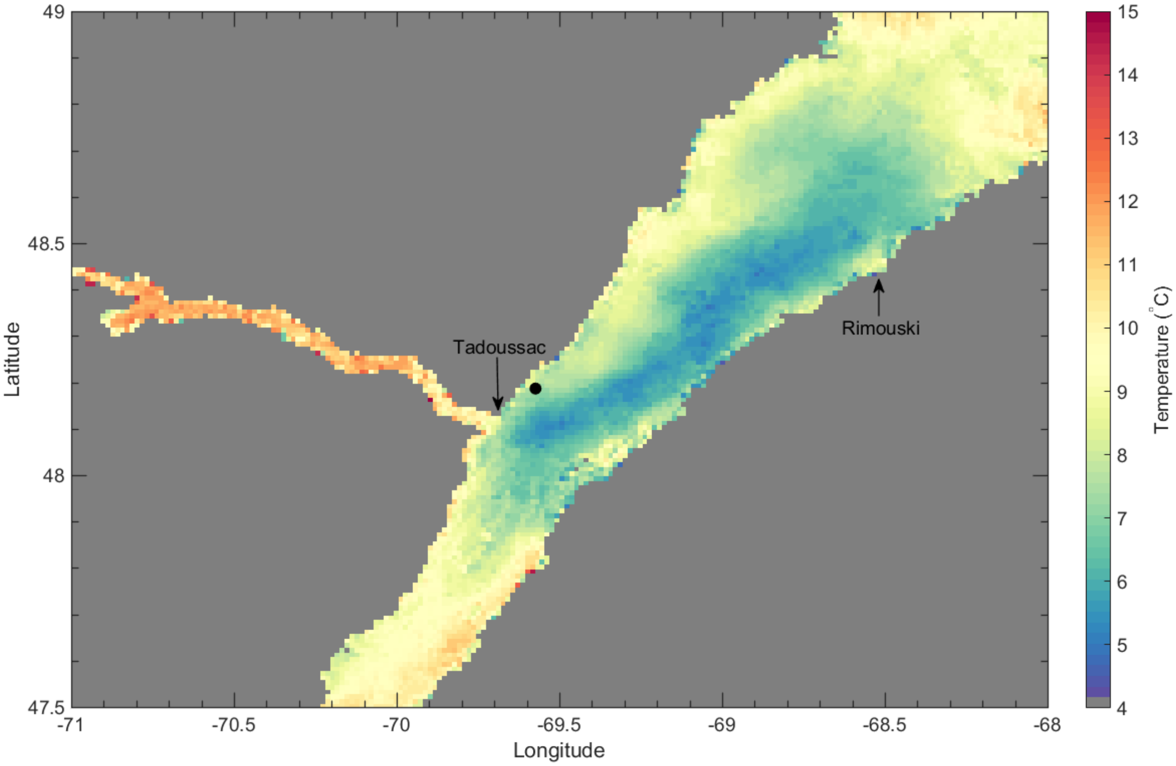

Figure 3. Three-day (June 13-15, 2013) average sea surface temperature during the fixed station (black dot) measurements (OGSL 2014).

Figure 4 -

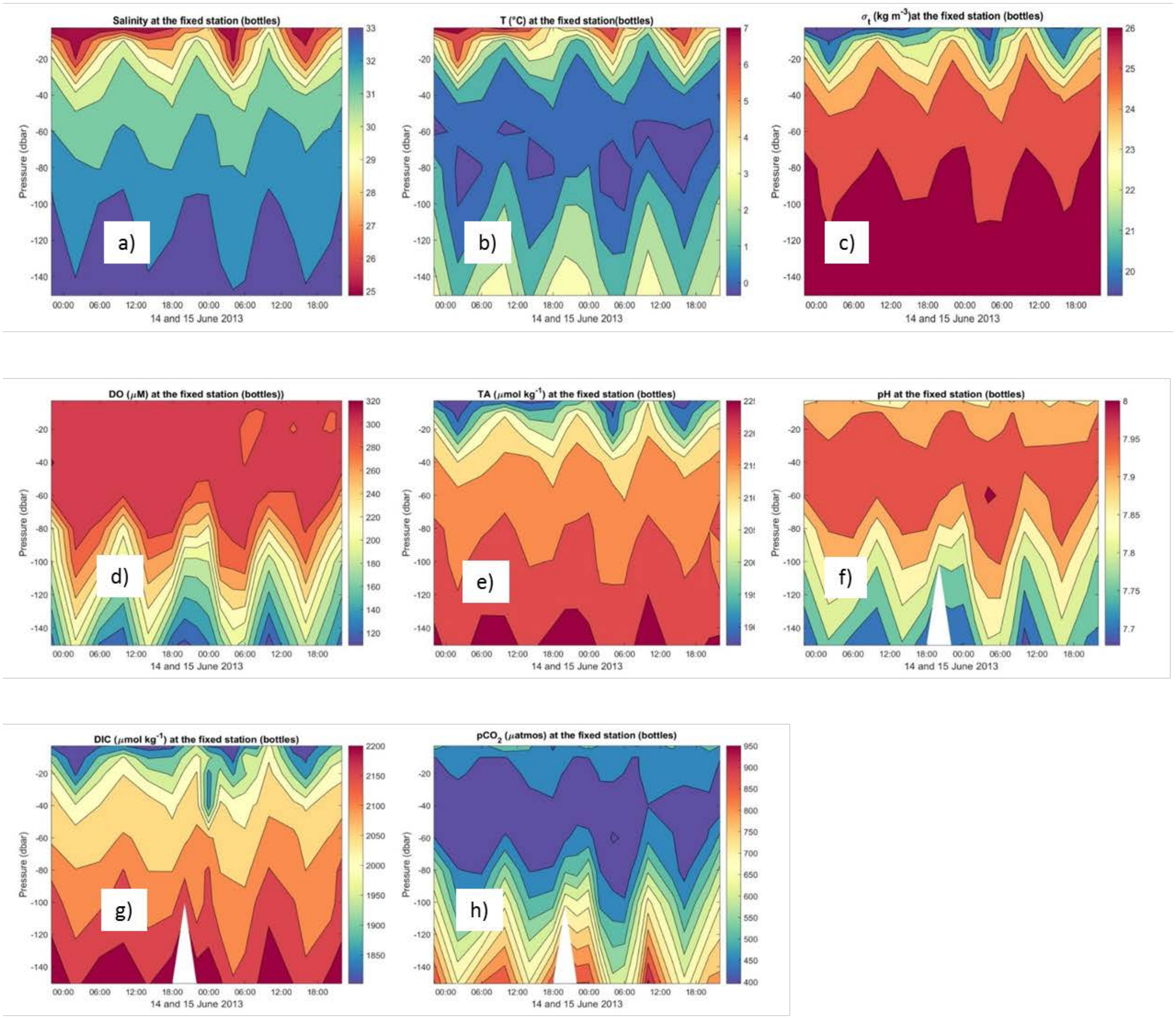

Figure 4. Water properties measured at the fixed station (48°11.2'N, 69°34.4'W) over two tidal cycles, June 14-15, 2013: a) Practical Salinity, b) Temperature, c) Sigma-t, d) Dissolved Oxygen, e) Titration alkalinity (TA), f) pH_T, g) Dissolved inorganic carbon (DIC, calculated from TA and pH_T), h) pCO_2 (calculated from TA and pH_T). All panels were plotted from discrete samples (~ 3, 10, 20, 40, 60, 80, 100 and 150 m) taken from the Niskin bottles. Dissolved nitrate, nitrite, silicate, and soluble reactive phosphate (SRP) data can be found in the electronic attachment.

Figure 5 –

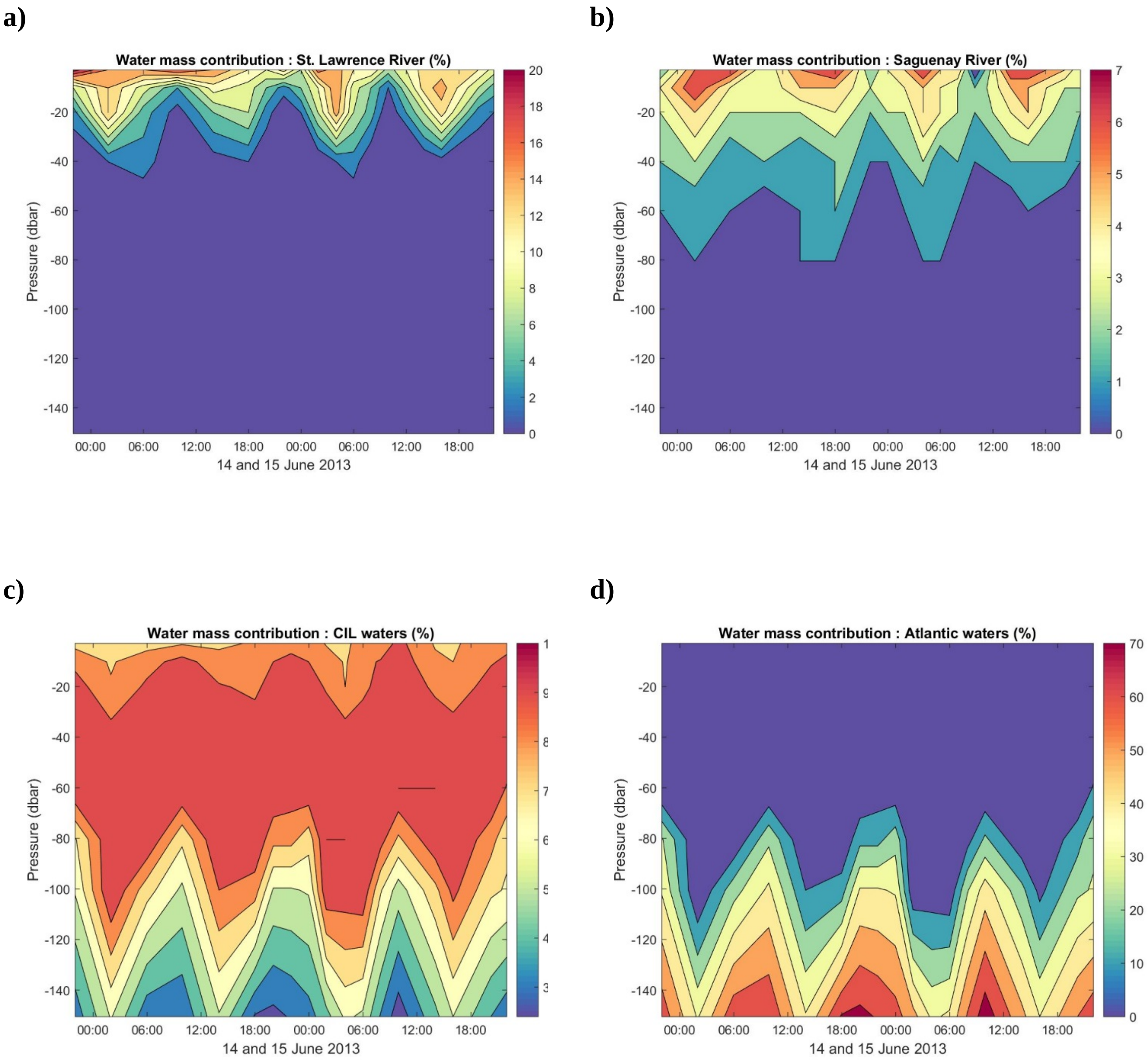

Figure 5. Distribution (%) of water-source types at the fixed station (48°11.2’N, 69°34.4’W) over two tidal cycles, June 13-15, 2013: a) St. Lawrence River water, b) Saguenay River water, c) cold intermediate layer (CIL) water, d) Lower St. Lawrence Estuary (LSLE) bottom water or Atlantic water.

Figure 6-

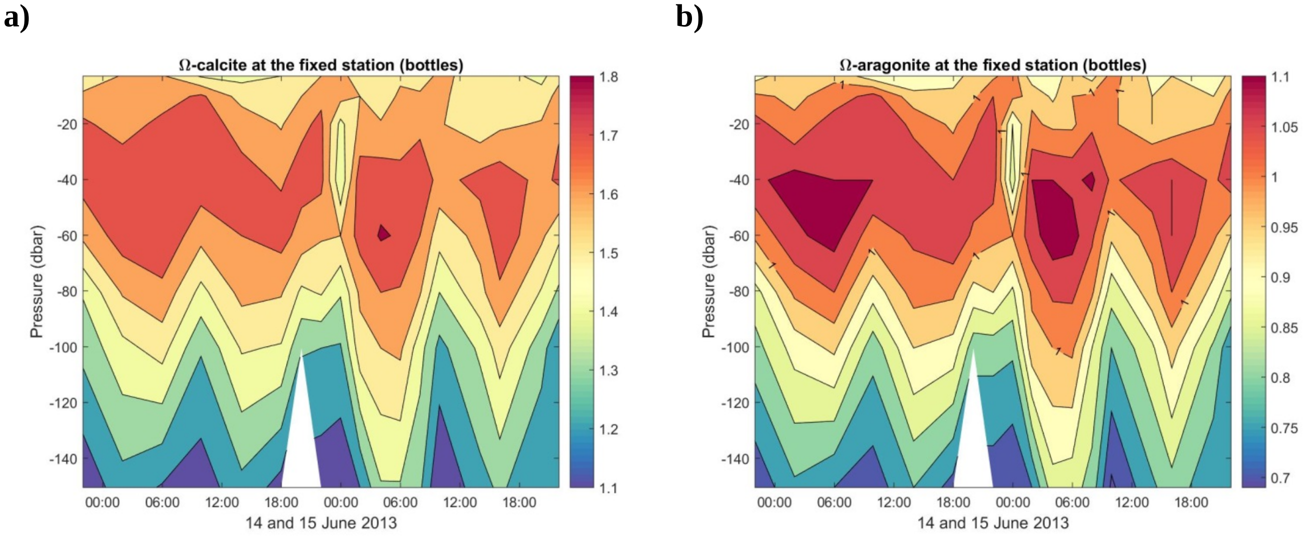

Figure 6. Saturation state of the water column with respect to a) calcite and b) aragonite at the fixed station (48°11.2’N, 69°34.4’W) over two tidal cycles, June 14-15, 2013.

Figure 7-

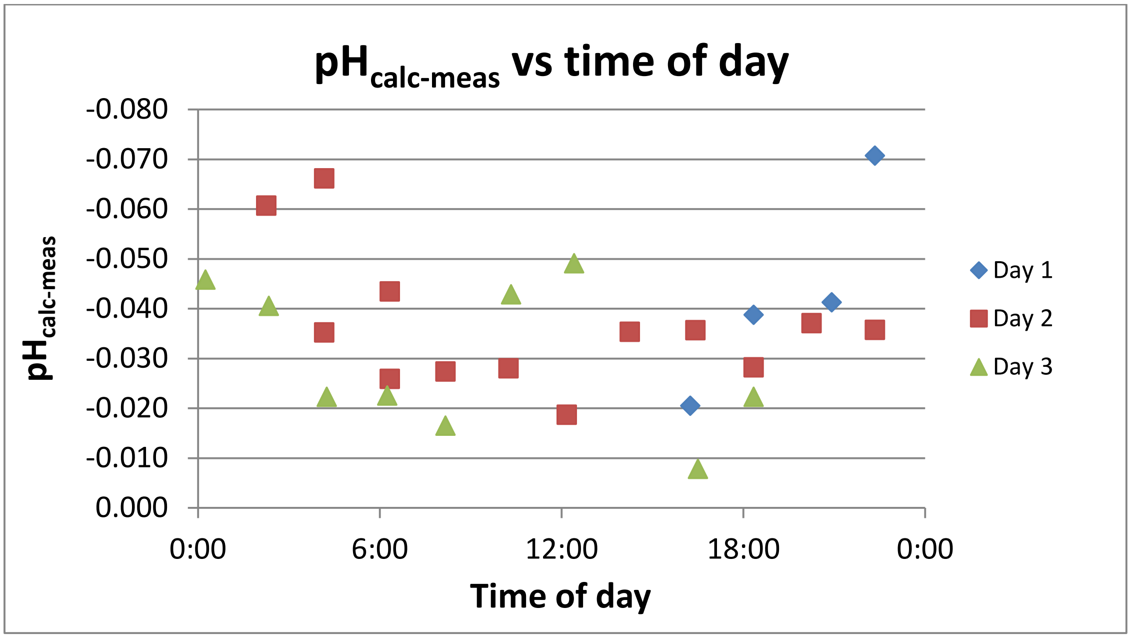

Figure 7 – Difference between calculated (based on conservative mixing of the four source water types) and measured pH_T values in the surface waters at the fixed station as a function of the time of day over two full tidal cycles over three consecutive days (see Table 2 for details). Errors originate mostly from the variance on the fractional contributions obtained from the OMP analysis and, in this specific situation on the fractional contribution of the Saguenay River water (most divergent TA and pH). Although typically on the order of 10% (Lansard et al. 2012), we applied a +50% error to this value and the difference in computed pH_T was less than 0.003 unit, below the uncertainty of our field measurements and smaller than the size of the symbols.

Table 1. Source water types and their characteristic properties used in the OMP analysis

Water types	T (°C)	S_P	δ^{18}O (‰)	TA ---(µmol kg^{-1})--	DIC[1]	DO -------- (µmol L^{-1}) -------	ΣSi	SRP	DIN	pCO_2 (µatm)	pH_t
St. Lawrence River	15	0	-9.61	1000	1022	300	45[2]	0.7[2]		575	8.11[3]
Saguenay River	12	0	-13.14	80	97	320	78[2]	1.2[2]		340	7.12[3]
CIL	-0.3	32.13	-1.64	2183	2108	295	10.5	1.1	9.8	450	7.97
LSLE Bottom water	5.2	34.51	-0.28	2296	2165	63.5	52.2	2.4	22.8	1400	7.62

TA – titration alkalinity, DIC – dissolved inorganic carbon, DO – dissolved oxygen,
ΣSi – dissolved silicate, SRP – soluble reactive phosphate, DIN – dissolved inorganic nitrogen

[1] DIC values were not measured directly, but calculated from pH and TA using the Excel version of CO2SYS (Pierrot et al., 2006) for the marine waters and the web-based version of PHREEQC (www.ndsu.edu/webphreeq/) for the freshwaters.

[2] Values were not measured at the time of sampling, they are averages of measurements carried out in the previous 5 years at similar times of the year.

[3] pH of freshwaters were not measured at the time of sampling, values that appear in the table are averages of measurements carried out in the previous 5 years at similar times of the year on the NBS scale (infinite dilution convention).

Table 2. Weight applied to each parameter used in the OMP analysis

Parameters	Precision	Weights used in OMP analysis Above the CIL	Below the CIL
Temperature (°C)	0.01	1	25
Practical salinity	0.01	25	25
Dissolved O_2 (µmol L^{-1})	2.0	1	5
Total alkalinity (µmol kg^{-1})	2.0	25	25
$\delta^{18}O(H_2O)$ (‰)	0.05	25	25
Mass conservation		25	25

Table 3. Reconstructed surface water properties at the fixed station (SF) (conservative mixing of source-water types according to the OMP results) over two full tidal cycles (June 13-15, 2013) and differences between the calculated and observed values.

Time	Depth	pH$_{T}$	DIN	SRP	ΣSi	DO	ΔpH$_{T}$	ΔDIN	ΔSRP	ΔSi	ΔDO
	(m)		--------- µmol/L --------					----------- µmol/L ----------			
16:15	3.2	7.833	13.5	1.06	18.5	297	-0.021	-5.1	0.21	-3.9	-10
18:20	3.1	7.840	13.6	1.02	19.0	297	-0.039	1.3	0.26	-2.6	-16
20:55	3.1	7.841	14.2	1.05	20.0	297	-0.041	-9.2	0.29	-1.6	-13
22:20	2.9	7.849	14.3	1.04	20.3	297	-0.071	5.4	0.28	-1.3	-14
1+ 0:10	3.2	7.856	13.9	1.04	19.6	297	-0.047	1.3	0.28	-2.0	-11
1+ 2:15	2.8	7.858	14.6	1.04	21.0	298	-0.061	-1.6	0.43	-0.9	-12
1+ 4:10	1.2	7.861	13.9	1.05	19.5	297	-0.066	8.8	0.44	-1.5	-4
1+ 4:10	3.1	7.889	12.9	1.09	17.1	297	-0.035	-14.8	0.47	-3.9	-9
1+ 6:20	1.3	7.840	14.6	1.04	20.9	297	-0.043	0.8	0.32	-0.7	-5
1+ 6:20	3.2	7.837	13.6	1.03	19.0	297	-0.026	-7.7	0.39	-2.0	-10
1+ 8:10	3.1	7.853	13.9	1.04	19.5	297	-0.027	-8.0	0.40	-1.5	-14
1+ 10:15	3.2	7.861	14.1	1.04	20.0	297	-0.028	-5.5	0.40	-1.3	-13
1+ 12:10	2.7	7.841	14.2	1.04	20.2	297	-0.019	-8.2	0.34	0.2	-14
1+ 14:15	2.8	7.904	13.9	1.06	19.4	297	-0.035	3.8	0.26	0.2	-10
1+ 16:25	3.0	7.886	12.9	1.06	17.1	297	-0.036	0.7	0.09	0.2	-5
1+ 18:20	3.5	7.885	12.4	1.05	16.3	296	-0.028		0.19	-3.3	-8
1+ 20:15	3.1	7.864	12.2	1.07	15.8	296	-0.037		0.14	-2.4	-11
1+ 22:20	3.0	7.861	13.8	1.04	19.3	297	-0.036	2.6	0.29	-3.3	-10
2+ 0:15	2.6	7.852	14.3	1.05	20.3	297	-0.046	-0.3	0.31	0.8	-13
2+ 2:20	2.9	7.880	13.1	1.06	17.7	297	-0.041	1.9	0.33	-3.2	-7
2+ 4:15	3.2	7.874	13.3	1.06	18.2	297	-0.022	-5.0	0.20	-0.3	-10
2+ 6:15	3.1	7.910	10.9	1.07	13.0	296	-0.023	11.3	0.06	-0.9	-5
2+ 8:10	3.3	7.856	12.5	1.06	16.4	296	-0.017	-5.4	0.14	-0.7	-8
2+ 10:20	3.3	7.847	14.2	1.05	20.0	298	-0.043	1.1	0.27	0.1	-9
2+ 12:25	3.2	7.861	14.3	1.05	20.2	298	-0.049	1.9	0.26	-0.1	-8
2+ 16:30	3.2	7.883	13.1	1.06	17.6	297	-0.008	-7.6	0.19	-2.3	-8
2+ 18:20	2.7	7.885	12.3	1.07	16.0	296	-0.022	-0.8	0.28	1.4	-7

Figure captions -

Figure 1. a) Map of the St. Lawrence Estuary and location of stations visited on a cruise immediately prior to this study (June 3-8, 2013) as well as b) the transect track and position of the fixed sampling station visited during this study (June 10-15, 2013). Water properties measured on the previous cruise and along the transect were used to define the water-type properties and served for the water mass analysis in OMP.

Figure 2. a) Vertical profiles of the salinity (red line) and temperature (blue line) throughout the water column as recorded at the fixed station on June 11, 2013 at 16:48 GMT. We also show the profiles (thick black lines) from station 18. The data are reproduced in a T-S diagram (b) that reflects the three-layer estuarine circulation in the Lower St. Lawrence Estuary.

Figure 3. Three-day (June 13-15, 2013) average sea surface temperature during the fixed station (black dot) measurements (OGSL 2014).

Figure 4. Water properties measured at the fixed station (48°11.2'N, 69°34.4'W) over two tidal cycles, June 14-15, 2013: a) Practical Salinity, b) Temperature, c) Sigma-t, d) Dissolved Oxygen, e) Titration alkalinity (TA), f) pH_T, g) Dissolved inorganic carbon (DIC, calculated from TA and pH_T), h) pCO_2 (calculated from TA and pH_T). All panels were plotted from discrete samples (~ 3, 10, 20, 40, 60, 80, 100 and 150 m) taken from the Niskin bottles.

Figure 5. Distribution (%) of water-source types at the fixed station (48°11.2'N, 69°34.4'W) over two tidal cycles, June 13-15, 2013: a) St. Lawrence River water, b) Saguenay River water, c) cold intermediate layer (CIL) water, d) Lower St. Lawrence Estuary (LSLE) bottom water or Atlantic water.

Figure 6. Saturation state of the water column with respect to a) calcite and b) aragonite at the fixed station (48°11.2'N, 69°34.4'W) over two tidal cycles, June 14-15, 2013.

Figure 7 – Difference between calculated (based on conservative mixing of the four source water types) and measured pH_T values in the surface waters at the fixed station as a function of the time of day over two full tidal cycles over three consecutive days (see Table 2 for details). Errors originate mostly from the variance on the fractional contributions obtained from the OMP analysis and, in this specific situation on the fractional contribution of the Saguenay River water (most divergent TA and pH). Although typically on the order of 10% (Lansard et al. 2012), we applied a +50% error to this value and the difference in computed pH_T was less than 0.003 unit, below the uncertainty of our field measurements and smaller than the size of the symbols.

Supplemental material –

Fig S1.

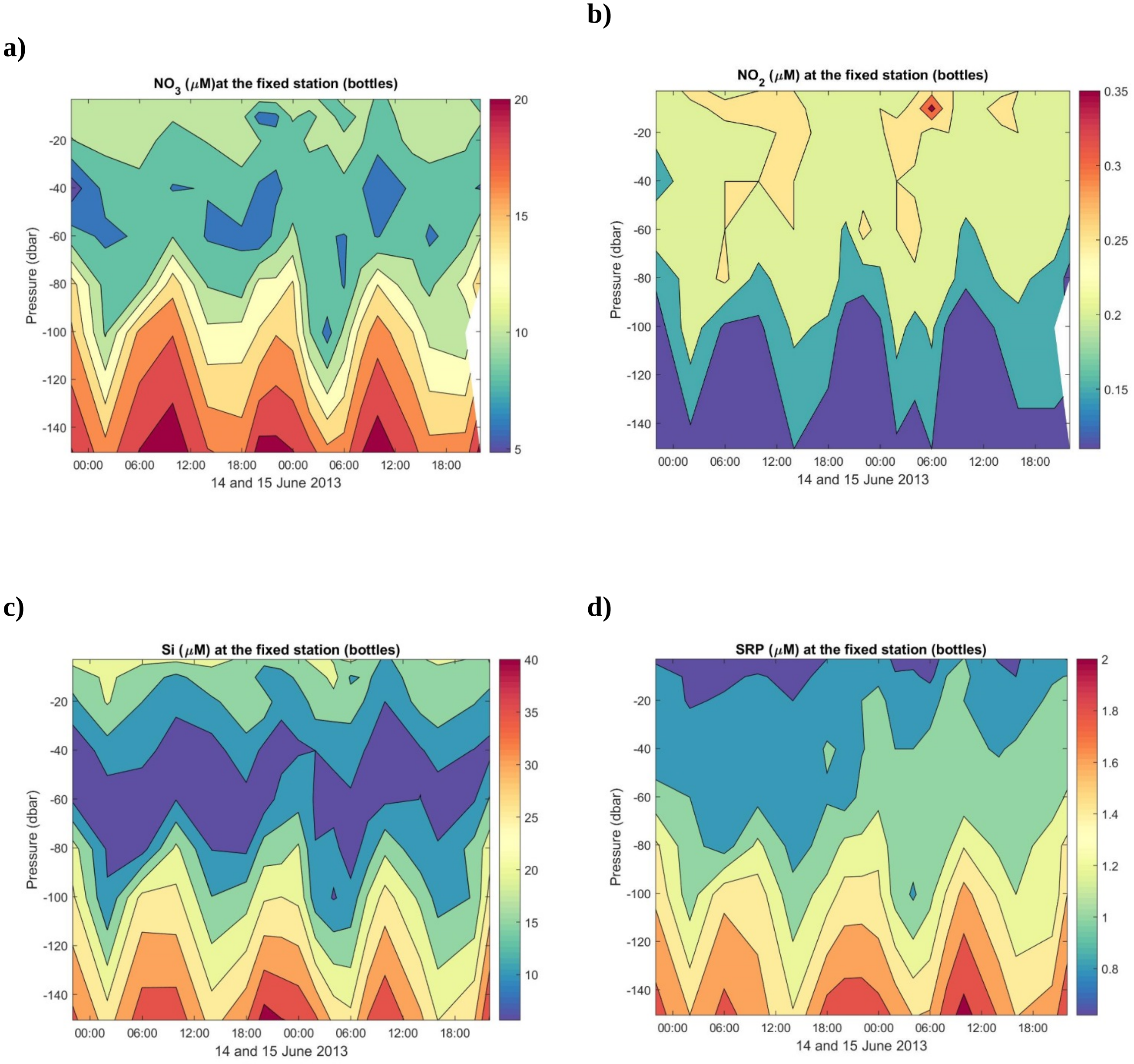

Figure S1. Water properties measured at the fixed station (48°11.2'N, 69°34.4'W) over two tidal cycles, June 14-15, 2013: a) Dissolved nitrate, b) Dissolved nitrite, c) Dissolved silicate, d) Soluble reactive phosphate (SRP). All panels were plotted from discrete samples (~ 3, 10, 20, 40, 60, 80, 100 and 150 m) taken from the Niskin bottles.